Ultrasonic evaluation of segmental variability in additively manufactured metal components

Manish Roy
Department of Electrical and Computer Engineering
University of Utah
Salt Lake City, United States
manish.roy@utah.edu

Kenneth Walton
Department of Chemical Engineering
University of Utah
Salt Lake City, United States
kenneth.walton@utah.edu

Joel B. Harley
Department of Electrical and Computer Engineering
University of Florida
Gainesville, United States
joel.harley@ufl.edu

Mikhail Skliar
Chemical Engineering and Nano Institute of Utah
University of Utah
Salt Lake City, United States
mikhail.skliar@utah.edu

***Abstract*— One of the primary challenges with additively manufactured metal components is the potential for the material heterogeneity, such as the variations in density, porosity, and elasticity. These heterogeneities are difficult to predict and can cause the deviation in material strength and structural reliability from the specified design. This paper presents a novel approach to the ultrasound characterization of spatially varying material properties and its application to a sample manufactured by the selective laser melting. The method is demonstrated for a 3D-printed aluminum alloy sample. The independent measurements of the elastic modulus, the surface morphology, and the X-ray computed tomography of the sample were consistent with the ultrasound results.**

Keywords*— *Additive Manufacturing, Selective Laser Melting, Ultrasonic Evaluation, Nondestructive Evaluation of Materials

I. INTRODUCTION

Selective laser melting (SLM) is an additive manufacturing process which deposits and melts metal powder layer-by-layer to produce intricate metal parts. The set-up cost for this method is relatively low, which makes it attractive for prototyping and low-volume fabrication. Complex geometries and internal structures, difficult to produce by traditional techniques, are readily amenable to the SLM manufacturing.

During SLM fabrication, some regions of the fabricated part are repeatably reheated as new layers are added. This thermal cycling history varies with the location and may cause microstructural heterogeneity, residual stresses, and spatial variation in mechanical properties, as was observed for a stainless-steel sample [1]. X-ray computed tomography (CT) can characterize microstructure heterogeneity, but there is no technology to characterize the internally varying mechanical properties.

Traditional nondestructive ultrasound evaluation provides an aggregate characterization of mechanical properties and is insensitive to their spatial variability. This paper adapts the previously developed method for the ultrasound measurements of the segmental temperature distribution (US-MSTD) in solids [2–4] to estimate the spatial variability of mechanical properties in SLM-manufactured parts.

The speed of sound in solids, v, depends on the material's Young's modulus, E, Poisson's ratio, μ, and density, ρ:

$$v = \sqrt{\frac{E(1-\mu)}{\rho(1+\mu)(1-2\mu)}} \quad (1)$$

For thin rods, this relationship simplifies to the following form:

$$v = \sqrt{\frac{E}{\rho}} \quad (2)$$

The measured speed of sound (SOS) is, therefore, sensitive to E, μ, and ρ and their spatial variability along the length of the ultrasound propagation. In the pulse-echo mode, by measuring the time of flight (TOF), t_{of}, of an excitation pulse across the sample of the length L, the speed of sound is obtained as:

$$v = \frac{2L}{t_{of}} \quad (3)$$

While v obtained this way will indicate changes in the material properties along the path of propagation, it is not possible to identify the regions where the variations are localized.

This challenge of ultrasonic characterization of spatially distributed properties was previously addressed for temperature distribution measurements by the US-MSTD method. This approach resolves the lack of unique dependence of the SOS on the temperature distribution by using a structured propagation path with multiple echogenic features that are engineered to create a train of ultrasound echoes from known locations. The TOF of each echo in the train encodes the temperature distribution in different segments.

In this work, building on the central idea of the US-MSTD method, we measured the segmental speed of sound in a 3D-printed 31AL aluminum alloy sample. The segmentation was performed by incorporating internal echogenic features into the sample during its SLM fabrication. The SOS in all segments was found to be approximately the same, which indicates that in our experiments the difference in thermal processing history during SLM did not induce changes in material properties detectable by the ultrasound measurements.

The independent measurements of the elastic modulus, the surface morphology of different metal surfaces, and the X-ray CT of the sample were consistent with the ultrasound results. Overall, the preliminary results reported here indicate the feasibility of detecting heterogeneity of the material properties in 3D-printed parts following the developed approach. Further studies with compositionally complex (e.g., stainless steel) samples, for which thermal-cycling-induced heterogeneity was previously reported, are still needed.

The authors acknowledge financial support from the NETL of the U.S. Department of Energy under award number DE-FE0031559.

II. METHOD

A. 3D Printed Sample

A cylindrical part (30 mm diameter) was fabricated by selective laser melting (DMLM machine model Mlab cusing, Concept Laser GmbH) of aluminum powder (~90% Al and 10% Si, grade 31AL). The layer-by-layer melting of the powder by laser rastering which followed the computer-aided design (Fig 1B and video [5]) was repeated until an approximately 50 mm-long sample, shown in Fig. 1B, was completed. Three echogenic features divided the sample into four segments – S1, S2, S3, and S4 (Fig. 1C). Each centerline-located feature is a spherical region 2 mm in diameter where the powder was not melted during the manufacturing.

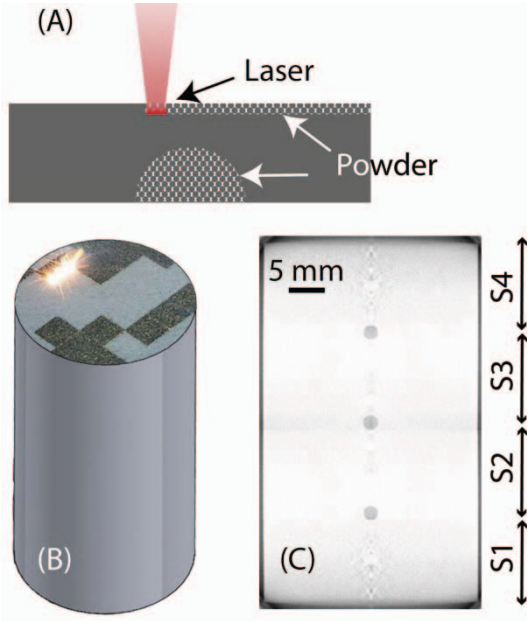

Fig. 1. (A) A cross-sectional view of the SLM process in action shows a layer of powder being melted by a laser beam. An echogenic feature below the surface is shown as a region of unmelted powder. (B) The part emerges as new layers are added. The rastering pattern of the laser beam melting a new layer is shown as a screen caption from the video [5]. (C) The acquired X-ray CT image of the fabricated sample shows internal echogenic features as gray circles. The internal echogenic features appear in the image as gray circles, which indicates lower-density regions of unmelted powder.

B. Ultrasound Measurements

The square-wave pulser/receiver (model 5077PR, Olympus IMS, Waltham, MA) was used to send an excitation pulse to an ultrasound transducer (5 MHz central frequency, 0.5" diameter, protected face; model v609 RB from Panametrics, Waltham, MA), which was coupled to the flat base of the described 3D-printed cylindrical aluminum sample. The received echoes were digitized by a mixed signal oscilloscope (Tektronix MSO 2024) and saved for signal analysis.

Fig. 2A shows the echoes produced by proximal and distal ends (PE and DE) of the sample and the three echogenic features (EF1, ..., EF3). This time series, $y(t)$, was obtained by averaging 30 raw signals acquired from the oscilloscope at the identical experimental conditions. Segment S1, ..., S4 are bounded by PE, EF1, ..., EF3, and DE (Fig. 1C). The segmental lengths and the corresponding TOF across each segment are used in equation (3) to calculate the segmental SOS.

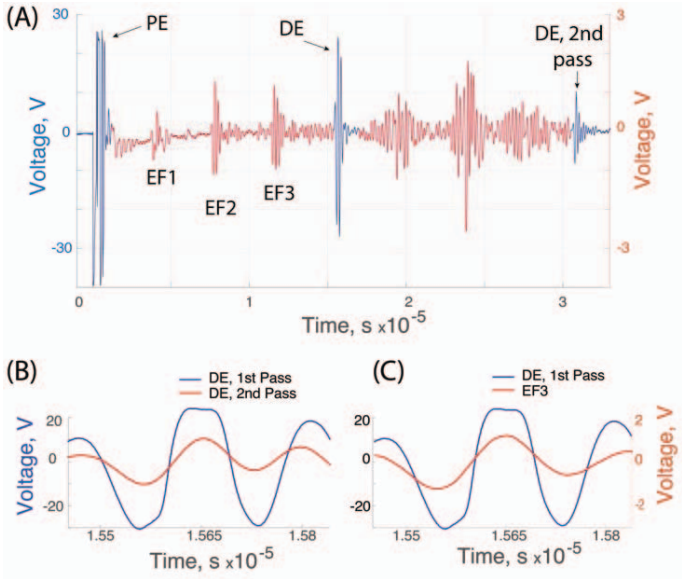

Fig. 2. (A) The waveform $y(t)$ shows echoes produced after two passes (round trips) of the excitation pulse through the sample. Each pass results in four echoes: The echogenic features (EF1–3) produce three echoes, and the fourth one is reflected from the distal end (DE) of the sample. The data were acquired at two different spans. A narrower span was used to record echoes from internal echogenic features (shown in red). (B) Cross-correlation between echoes reflected from the distal end after the first and the second pass of the pulse through the sample. (C) Cross-correlation of the echoes from the distal end and the echogenic feature EF3.

C. Segmental TOF

First, the data windows containing all echoes of interest were identified within the waveform $y(t)$, Fig. 2A. To identify an echo, the envelope of the waveform was calculated [6,7] and convolved with the Gaussian kernel ($\sigma = 1.4$). The peaks produced by the convolution marked the location of each echo within the time series $y(t)$. The data windows indexed by the peak locations were extracted from $y(t)$ and cross-correlated in time domain to determine the time difference between the echoes.

The cross-correlation between the echoes reflected from the distal end (DE) of the sample after one and two passes of the excitation pulse through the sample was used to find the total TOF through the sample, t_{of}^{Sample}.

Fig. 2B overlaps the two waveforms after shifting the second-pass echo by $t_{of}^{Sample} = t_{of}^{DE,\text{2nd pass}} - t_{of}^{DE}$. Fig. 2C superimposes the 1st-pass DE echo with the echo produced by the third echogenic features EF3, which was shifted by the time difference determined by the described cross-correlation procedure.

As the second step, the segmental TOF was calculated as the time difference between different echoes. For example, t_{of}^{S2}, which is the TOF through segment S2, was calculated as the difference between the arrival time of echoes produced by the 2nd and the 1st echogenic features, t_{of}^{EF2} and t_{of}^{EF1}:

$$t_{of}^{S2} = t_{of}^{EF2} - t_{of}^{EF1} \quad (4)$$

Similarly, $t_{of}^{S3} = t_{of}^{EF3} - t_{of}^{EF2}$ and $t_{of}^{S4} = t_{of}^{DE} - t_{of}^{EF3}$. The waveform produced by the "initial bang" at the proximal end of the sample is very different from other echo waveforms and was not used in the calculation of the TOF through segment S1. Instead, t_{of}^{S1} was found as:

$$t_{of}^{S1} = t_{of}^{Sample} - \sum_{i=2}^{4} t_{of}^{Si} \quad (5)$$

D. Segmental Lengths

The overall length of the sample, L, was measured with a micrometer, which imposed the constraints on the sum of the individual segments, L_{Si}: $\sum_{i=1}^{4} L_{Si} = L$. The length of segments S2 and S3 were obtained from the distance between internal echogenic features, as imaged by a microCT. Each echogenic feature had the same shape and size, as shown in Fig. 1C. Based on the measured segmental TOF and lengths, the speed of sound in S2 and S3 was calculated and found to be essentially the same (differed by less than 4 m/s, which corresponds to 0.0713% difference in the SOS).

Segments S1 and S4 are bound by dissimilar features: the flat circular bases of the cylindrical sample and internal echogenic features EF1 and EF3, respectively. Therefore, we elected to estimate their lengths using their segmental time of flights and then compare the results for the consistency with the microCT imaging.

Fig. 3 illustrates the procedure for estimating L_{S1} and L_{S4}. A line with the slope equal to the inverse of the SOS in segments S2 and S3 was drawn through a point defined by the length of the ultrasound propagation through the sample ($= 2L$) and the time-of-flight through the sample, t_{of}^{Sample}. The TOF through the first segment and the line in Fig. 3 were then used to determine the corresponding value of L_{S1} and L_{S4}.

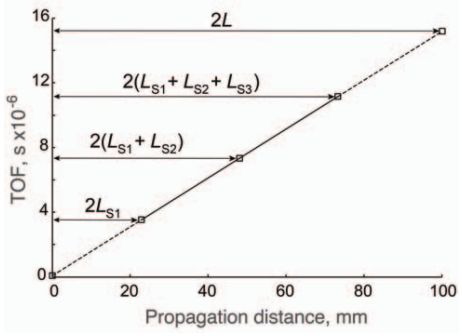

Fig. 3. The inverse of the speed of sound in segments S2 and S3, SOS^{-1}, is used as the slope of the line drawn through the boxed point $(2L, t_{of}^{Sample})$ defined by the total length of the sample and the TOF through it. The other three boxed points on the line are determined by the cumulative TOFs across the segments of the sample: t_{of}^{S1}, $t_{of}^{S1} + t_{of}^{S2}$, and $t_{of}^{S1} + t_{of}^{S2} + t_{of}^{S3}$.

E. Imaging and Mechanical Characterization of the Sample

The X-ray microCT imaging of the 3D-printed aluminum sample by X-ray microscope (XRadia Micro XCT 400, Carl Zeiss X-ray Microscopy, Pleasanton, CA) was performed to noninvasively characterize the size and the locations of the introduced internal echogenic features. X-rays were generated by a beam of electrons accelerated by 10.0 kV voltage applied to the X-ray tube. At this condition, a 40-micron spatial resolution is achieved. Two scans, processed using Xradia XMReconstructor, were needed to image the entire sample. The single image shown as Fig. 1C was obtained by stitching the results of the two scans in ImageJ. Small centerline features and diffused edges, which can be seen in Fig. 1C, are imaging artifacts.

After completing the ultrasound characterization, we mechanically polished the flat surfaces (top and bottom) of the sample and imaged the surface topography by secondary and backscatter electrons. The scanning electron microscope (SEM, FEI Quanta 600 FE-SEM) was operated at 20.0 kV with spot size set to 5, the magnifications between 1,000-4,000×, and the 9.1 mm distance between the imaged surface and the detector.

The top and bottom surfaces of the sample, processed at the beginning and the end of the SLM fabrication, experienced a very different thermal processing history, with the bottom layer undergoing repeated re-heating as new layers are added, whereas the top layer is heated just once. We characterized the impact of processing history on the mechanical properties of the material adjacent to the top and bottom surfaces of the SLM-fabricated sample using the nanoindenter (Hysitron TI Premier, Bruker, Billerica, MA). The instrument was outfitted with a diamond probe used to indent the surface of the material. The force-displacement curve during the indentation was recorded and provided the information from which the reduced modulus and the hardness of the material in different locations on the top and bottom surfaces of the sample were obtained.

III. RESULTS

The described analysis was applied to the data provided by the CT image and the ultrasound waveform $y(t)$ to determine the length of each segment and the segmental time-of-flight. The obtained values were then used to calculate the segmental speed of sound. Table I summarizes the results.

The results in Table I are specific the waveform depicted in Fig. 2A, which was acquired when the ultrasound transducer was coupled to one of the flat surfaces of the sample (Face 1). After changing the orientation of the transducer by coupling it to the other flat surface of the sample (Face 2), a different ultrasound waveform was obtained (not shown) and analyzed. Table II lists the results obtained in this transducer orientation.

TABLE I. SEGMENTAL DATA FOR INCIDENT FACE 1

Segments	***S1***	***S2***	***S3***	***S4***	***Overall***
Length, mm	11.4750	12.5654	12.6259	13.4037	50.07
TOF, µs	3.46505	3.79670	3.81227	4.04797	15.12198
SOS, m/s	6,623.28	6,619.11	6,623.82	6,622.43	6,622.15

The examination of data in Tables I and II indicates that, while the lengths of S2 and S3 remain consistent irrespective of the transducer orientation, the lengths of segments S1 and S4 are not. As orientation is revered, so does the length of S1 and S4, but the sum remains the same: $L_{S1} + L_{S4} = 24.8787$ mm. We interpret this result to imply that the reflection of the ultrasound wave primarily occurs from the leading apex of spherical echogenic features. For Face 1 orientation, the length of S1 is the distance between the proximal surface and the point on the echogenic feature EF1 the closest to the transducer. On the

other hand, L_{S4} is the distance between the point on the surface of EF4 closest to the transducer and the distal surface of the sample. Therefore, for the equally spaced and identical in size echogenic features, L_{S4} should be larger than L_{S1} by 1 diameter of an echogenic feature. Indeed, inspecting Table I we see that L_{S4} is larger than L_{S4} by ~2 mm, which is the diameter of the echogenic features determined from the microCT image. The situation is reversed when the transducer is attached to Face 2.

TABLE II. SEGMENTAL DATA FOR INCIDENT FACE 2

Segments	***S1***	***S2***	***S3***	***S4***	***Overall***
Length, mm	13.2283	12.6259	12.5654	11.6504	50.07
TOF, µs	3.99460	3.79990	3.79997	3.51209	15.10656
SOS, m/s	6,623.09	6,645.38	6,613.42	6,634.44	6,628.91

The comparison of Tables I and II shows that even though L_{S1} and L_{S4} change with the transducer orientation, the speed of sound in segments S1 and S4 remain approximately the same due to the corresponding change in the time-of-flight.

An essentially constant SOS listed in both tables indicates that the mechanical properties were unaffected by the difference in thermal cycling during the manufacturing.

Independent characterization techniques were used to confirm the validity of this conclusion. Specifically, the density variation was not evident in X-ray microCT images. The surface morphology, imaged by the SEM (Fig. 4), was similar for both faces. However, surface pores with the characteristic size of less than 5 µm were more prevalent on the face not subjected to multiple reheat cycles. The increased porosity in the top layer may be explained by the local variations in metal powder packing density, leading to the localized variation in metal thickness upon melting which, for the top layer, is not remedied by the deposition of subsequent layers. The processing conditions are also known to contribute to the formation of pores in aluminum alloy parts manufactured by the SLM [8]. Finally, the mechanical properties of the material were measured directly using the force-displacement data acquired during nanoindentation of the two flat surfaces of the sample. On each surface, measurements in multiple locations were acquired, averaged, and summarized in Table III as a mean plus-minus standard deviation. The small difference in mean values was not statistically significant.

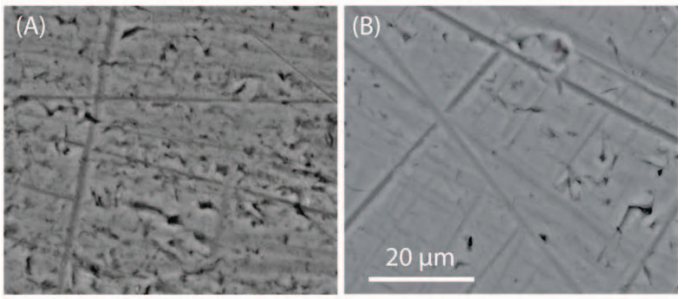

Fig. 4. The SEM images (2,000× magnification) formed by backscattered electrons reveal dissimilar pore density on the surfaces subjected to different thermal cycling history.

TABLE III. NANOINDENTER RESULTS

	Incident Face 1	**Incident Face 2**
Average Reduced Modulus, GPa± Std	83.08±13.69	85.79±10.19

IV. CONCLUSION

In this paper, we developed a novel approach to the ultrasound characterization of spatially varying material properties and applied it to a sample manufactured by the selective laser melting. Additive manufacturing of metal components from metallic powder by computer-controlled SLM allows the production of monolithic parts with complex geometry, the optimized design, which may not be achievable with conventional manufacturing techniques, and low cost. However, for the SLM-fabricated parts, the thermal cycling history varies with the location, which was reported to cause the spatial heterogeneity in mechanical properties in a stainless-steel sample [1].

To perform the ultrasonic characterization of spatially distributed material properties, we measured the segmental speed of sound in a 3D-printed 31AL aluminum alloy sample. The segmentation was achieved by incorporating internal echogenic features into the sample during its SLM fabrication. The SOS in all segments was found to be approximately the same, which indicates that in our experiments the difference in thermal processing did not induce detectable changes in material properties. The independent measurements of the elastic modulus, the surface morphology, and the X-ray CT of the sample were consistent with the ultrasound results.

The experiments reported in this paper indicate the feasibility of detecting heterogeneity of the material properties in 3D-printed parts following the developed approach. Further studies with samples, for which thermal-cycling-induced heterogeneity was previously reported, are currently underway.

REFERENCES

[1] Y. Liu, Z. Pang, and J. Zhang, “Comparative study on the influence of subsequent thermal cycling on microstructure and mechanical properties of selective laser melted 316L stainless steel,” Appl. Phys. A, vol. 123, no. 11, p. 688, November 2017.

[2] Y. Jia, V. Chernyshev, and M. Skliar, “Ultrasound measurements of segmental temperature distribution in solids: Method and its high-temperature validation,” Ultrasonics, vol. 66, pp. 91–102, March 2016.

[3] Y. Jia and M. Skliar, “Noninvasive ultrasound measurements of temperature distribution and heat fluxes in solids,” Energy and Fuels, vol. 30, pp. 4363–4371, no. 5, May 2016.

[4] M. Skliar, K. Whitty, and A. Butterfield, "Ultrasonic temperature measurement device," US Patents 8,801,277 B2, 2014, and 9,212,956, 2015.

[5] https://www.youtube.com/watch?v=ngtttSZ7bpg&feature=youtu.be.

[6] J. Dugundji, “Envelopes and pre-envelopes of real waveforms,” IRE Transactions on Information Theory, vol. 4, no. 1, pp. 53–57, Mar. 1958.

[7] Y. Jia and M. Skliar, "Anisotropic diffusion filter for robust timing of ultrasound echoes," 2014 IEEE International Ultrasonics Symposium, Chicago, IL, 2014, pp. 560-563.

[8] N. T. Aboulkhair, N. M. Everitt, I. Ashcroft, and Chris Tuck, "Reducing porosity in AlSi10Mg parts processed by selective laser melting," Additive Manufacturing, vol. 1–4, pp. 77-86, October 2014.